Chapter 2
Fast Electrochemical Impedance Spectroscopy

EIS is a widely adopted method for the characterisation and diagnostics of electrochemical devices [1–5]. The impedance characteristic is measured at a fixed operating point defined by current I_{dc}. The conventional EIS approach utilises a sinusoidal waveform as an excitation signal (i.e., single-sine approach) [6, 7]. In order to measure the impedance in a frequency band of interest at frequencies $f_i \in \Omega$, the procedure of applying single-sine electric current excitation has to be repeated multiple times for each frequency f_i. Assuming linearity of the electrochemical device's dynamics around a fixed operating point, the device responds with sinusoidal voltage change with the same frequency f_i and particular amplitude and phase. The impedance of the electrochemical device at frequency f_i is the ratio between voltage and current in the frequency domain. Commonly, the transformation from time to frequency domain is performed by fast Fourier transform (FFT). Consequently, the impedance is the ratio between the complex FFT coefficients.

With the single-sine excitation approach, the impedance characteristic of an electrochemical device is constructed at discrete frequencies $f_i \in \Omega$. The approach provides precise impedance measurements because all of the energy of the excitation signal is condensed at a single frequency only. Such an excitation provides maximal perturbation at the selected frequency f_i at the expense of lengthy measurements.

Despite the simplicity of the excitation and the signal processing step, performing EIS with such an approach is inefficient. First, applying single-sine excitation signals is time consuming, which is tightly linked to the lower frequency limit of the frequency band. Secondly, the application of FFT as a signal processing tool provides solely time average impedance estimates thus failing to provide any additional information required for further processing, for instance confidence intervals. Consequently, there is an apparent need for an improved EIS approach that will allow shorter measurement time while at the same time providing richer output than simply time-averaged values.

P. Boškoski et al., *Fast Electrochemical Impedance Spectroscopy*,
SpringerBriefs in Applied Sciences and Technology,
DOI 10.1007/978-3-319-53390-2_2

Addressing these two issues, this chapter presents an approach based on DRBS as an excitation signal and CWT with Morlet mother wavelet as a signal processing tool. The DRBS is well-established as an excitation signal in the field of system identification since it has white-noise-like spectral properties in a predefined frequency band. The main advantage of using DRBS as excitation compared to the conventional one, is shorter probing time. Furthermore, with properly tuned parameters, CWT provides optimal time-frequency resolution. Consequently, it provides reliable impedance measurements along the entire frequency band. Additionally, it yields statistical information about confidence intervals of the impedance measurements.

The application of a more complex excitation signal, such as the proposed DRBS, offers several advantages. First, the time required for performing EIS is significantly shorter.[1] Secondly, as the electrochemical device is perturbed by the broadband signal, the value of impedance can be computed at any frequency of interest by properly adjusting the parameters of CWT and DRBS. Additionally, the frequency-domain representation of the Morlet wavelet exists in a closed form, therefore the required time-domain convolution can be efficiently conducted in the frequency-domain as a multiplication. This implies a significant practical advantage for the implementation of the algorithm on embedded systems, where the computation resources are limited.

Employing the fast EIS technique in the optimal manner requires proper tuning of the CWT parameters. Additionally, DRBS excitation is usually implemented as a PRBS whose parameters also affect the overall performance of the fast EIS technique. For PRBS, these parameters include the order n, sampling period Δt, and amplitude a. For the CWT with the Morlet mother wavelet, the key parameters are the length of the signals, central frequency ω_0, cone of influence e. In what follows, methods for optimal parameter selection and computationally efficient implementation of the proposed fast EIS technique are presented.

2.1 Discrete Random Binary Sequence

The fundamentals of the DRBS origin from *continuous-time random binary signal* has the following two properties:

- the value of the signal can either be a or $-a$, and
- switch from one value to the other can occur at any given time.[2]

However, for the implementation and signal processing by means of digital computers, the *discrete random binary sequence* is much more convenient. In contrast to the continuous-time random binary signal, the changes in value of the discrete one occur only at discrete points in time $k\lambda$ ($k \in \mathbb{N}^0$), where λ is the length of the time interval. Time interval λ is the time between two consecutive points where the signal

[1] For detailed comparison see results presented in Sect. 4.4.

[2] In a given period of time, the probability of the number of changes of the signal's value is distributed according to Poisson distribution [8, pp. 161–162].

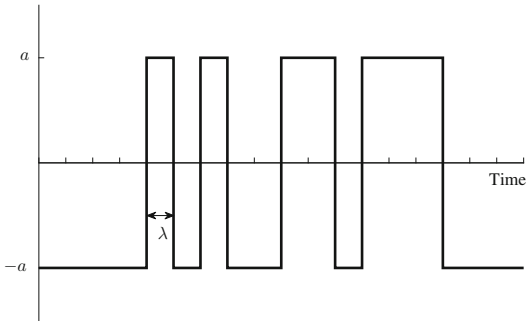

Fig. 2.1 DRBS waveform

can change its value. The generating process for DRBS has the following form:

$$X(t) = \sum_n a_n p(t - n\lambda - \alpha), \alpha \sim \mathscr{U}[0, \lambda], \tag{2.1}$$

where $p(t)$ is the probability describing the binary change of amplitude a and α is random phase shift, making process $X(t)$ stationary. A single realisation of the DRBS defined by (2.1) is shown in Fig. 2.1.

The power spectral density of the DRBS defined by (2.1) is

$$\Phi_X^d(\omega) = a^2\lambda \left| \frac{\sin\left(\frac{\omega\lambda}{2}\right)}{\frac{\omega\lambda}{2}} \right|^2. \tag{2.2}$$

The power spectral density shown in Fig. 2.2 has zeros exactly at integer multiples of the frequency $1/\lambda$. Since the beneficial properties of the DRBS are present only in a limited frequency band, the signal has to be applied with care. Out of this band, the device under examination is perturbed with substantially lower energy and thus it can not be characterised (identified) with sufficient accuracy. The useful frequency

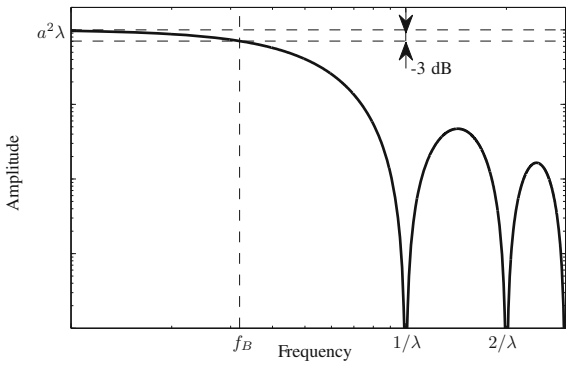

Fig. 2.2 Power spectral density of the DRBS

band f_B is approximately determined by the -3 dB frequency limit as [9]

$$f_B = \frac{1}{3\lambda}. \tag{2.3}$$

Pseudo-Random Binary Sequence

Mainly due to the ease of implementation, the PRBS is most often employed as a sufficiently close approximation of the DRBS. According to Ljung [10], PRBS is a periodic and deterministic signal with white-noise-like properties. As such, it is highly appropriate as an input test (i.e., excitation) signal for system identification purposes.[3] The maximum length PRBS is generated by employing feedback shift registers [8, 9]. The PRBS is characterised by

- the amplitude a, and
- the order n of the shift register,
- the length of the time interval λ.

The order n of the underlying shift register determines the maximum length N of the PRBS. In other words, it determines the number of discrete points in time when the PRBS signal can change its value. The relation between the order and the maximum length is as follows:

$$N = 2^n - 1. \tag{2.4}$$

Order n, together with the length of the time interval λ, defines the maximum length period T_p of the PRBS:

$$T_p = (2^n - 1)\lambda = N\lambda. \tag{2.5}$$

The discrete power spectrum density Φ^d of the maximum length PRBS with amplitude a and maximum length N is

$$\begin{aligned} \Phi^d(m) &= a^2 - \frac{a^2}{N} \sum_{\tau_i=1}^{N-1} e^{-j\frac{2\pi}{N} m\tau_i} \\ &= \begin{cases} \frac{a^2}{N} & m = 0 \\ \frac{a^2(N+1)}{N} & 0 < m < N. \end{cases} \end{aligned} \tag{2.6}$$

Therefore, the power spectrum of a periodic PRBS with the length of the time interval λ is

$$\Phi^p\left(m\frac{2\pi}{N\lambda}\right) = \frac{1}{N}\Phi^d(m)\left|\frac{\sin\frac{m\pi}{N}}{\frac{m\pi}{N}}\right|^2. \tag{2.7}$$

The power spectral density can be obtained by dividing the power spectrum (2.7) by $1/T$ as

[3] From the *systems theory's* point of view, EIS is a system identification technique.

$$\begin{aligned}\Phi^d(\omega) &= \frac{T}{N}\Phi^d(m)\left|\frac{\sin\frac{m\pi}{N}}{\frac{m\pi}{N}}\right|^2_{\omega=\frac{2\pi m}{T}} \\ &= \lambda\Phi^d(m)\left|\frac{\sin\frac{\omega\lambda}{2}}{\frac{\omega\lambda}{2}}\right|^2.\end{aligned} \tag{2.8}$$

By letting $N \to \infty$, the periodic PRBS signal becomes a signal with properties of the DRBS. The relation (2.6) becomes

$$\Phi^d(m) = a^2. \tag{2.9}$$

As a result, the power spectral density of the PRBS (2.8) becomes the same as the power spectral density of the DRBS (2.2).

It should be noted that PRBS is generated through a deterministic state machine and as such it can be created without any random number generator. However, true random generators are not rareness anymore in present-day microprocessors and therefore one can directly employ DRBS. The remaining analysis is valid regardless of whether PRBS or DRBS is used as an excitation signal.

2.2 Frequency Analysis

The straightforward way of extracting impedance data from the signals is by calculating the ratio of the Fourier transform of the excitation electric current and the resulting voltage as [7]

$$Z(j\omega) = \frac{U(j\omega)}{I(j\omega)} = \frac{\mathscr{F}\{u(t)\}}{\mathscr{F}\{i(t)\}}. \tag{2.10}$$

The resulting complex impedance characteristic $Z(j\omega)$[4] is incomplete. The biggest deficiency when calculating impedance using (2.10) is the lack of variance i.e., a general estimation of confidence intervals. The Fourier transform provides only time averaged amplitude and phase for the calculated frequencies. This issue can be resolved by employing time-frequency signal processing methods.

2.3 Time-Frequency Analysis

Unlike Fourier analysis, which allows only time-averaged analysis, the time-frequency methods enable analysis in a two dimensional time-frequency

[4]Throughout this book, the symbol j is used instead of $i = \sqrt{-1}$, since in the area of electrical engineering the symbol i is established as a symbol for electrical current.

plane [11]. As a result, the signal's spectral evolution in time can be observed. Typical examples of such methods are short-Time Fourier transform, Wigner–Ville distribution, Wavelet transform, etc. The biggest challenge is achieving optimal time-frequency resolution.

Theoretically, in the time domain the signals can be regarded as having "infinite" time resolution, i.e., one can zoom infinitely many details at an arbitrary time moment, at a cost of having no information about the signal's frequency. The opposite is valid for the pure frequency analysis, where the signal's spectrum contains all the frequency components but is lacking information regarding the time of their occurrence and duration. It should be noted that, by performing digital signal processing, even these methods have limited resolution that is directly connected to the sampling frequency.

Time-frequency analysis methods are bound to a limited time-frequency resolution regardless of the sampling frequency. There is an upper limit for the time-frequency resolution depending on the algorithm and its parameters. Therefore, the main goal is to determine the most suitable signal processing algorithm with such parameters that will result in optimal time-frequency resolution.

2.3.1 Short-Time Fourier Transform

A quite straightforward way of introducing time information bound to a particular spectrum is through the so-called short-time Fourier transform. It is defined as [12]

$$F(\tau, \omega) = \int_{-\infty}^{+\infty} f(t) w(t - \tau) e^{-j\omega t} dt, \tag{2.11}$$

where $w(t)$ is a window function. As such, (2.11) can be regarded as a time localised Fourier transform.

The selection of the window function $w(t)$ is the only parameter. The goal is to have a window function with good time and frequency localisation. The selection of the window and its duration defines the time-frequency resolution of the short-time Fourier transform. The main drawback of the short-time Fourier transform method is that this resolution is fixed.

2.3.2 Wavelet Transform

Wavelet transform resolves the problem of fixed time-frequency resolution by introducing the concepts of scaling a particular waveform with compact support called wavelets. A wavelet function $\psi(t)$ can be scaled and translated by introducing two parameters s and u as

$$\psi_{u,s}(t) = \frac{1}{\sqrt{s}} \psi \left(\frac{t - u}{s} \right). \tag{2.12}$$

CWT of a square integrable function $f(t) \in \mathbf{L}^2(\mathbb{R})$ is defined as [12]

$$Wf(s,u) = \int_{-\infty}^{\infty} f(t)\psi_{u,s}^*(t)\,dt, \tag{2.13}$$

where $\psi_{u,s}(t)$ is defined by (2.12).

Similarly, like the short-time Fourier transform, CWT also offers a way of time-frequency analysis but with adjustable time-frequency resolution. The wavelet coefficients (2.13) depend on the time and frequency characteristics of the function $f(t)$ in the region where the energy of the mother wavelet $\psi_{u,s}(t)$ is concentrated. This region can be described as a rectangle with fixed area, with size scaled with $1/s$.

Strictly speaking, the CWT transform (2.13) describes the analysed signal $f(t)$ on the time-scale plane. The conversion between scale s and actual frequency f is straightforward and depends on the selection of the mother wavelet, the only design parameter in this approach. Each scaling s alters the time-frequency resolution of the mother wavelet. High frequency resolution is preserved for lower frequencies, whereas high time resolution is preserved for higher frequencies.

2.3.3 The Morlet Wavelet

Similarly, like the selection of the window function for the short-time Fourier transform, the selection of the mother wavelet $\psi(t)$ significantly affects the performance of the CWT for the task at hand. In the context of EIS, both amplitude and phase are required. Therefore, the suitable mother wavelet should belong to the family of complex wavelets. Among several choices, two mother wavelets stand out: the Morlet wavelet and the Lognormal wavelet. Generally, it is regarded that the Morlet wavelet offers the optimal time-scale (frequency) resolution [13].

The Morlet wavelet is defined as [14]

$$\psi(t) = \pi^{-\frac{1}{4}} \left(e^{-j\omega_0 t} - e^{-\frac{\omega_0^2}{2}} \right) e^{-\frac{t^2}{2}}, \tag{2.14}$$

where ω_0 is referred to as the wavelet's central frequency and is usually set to a value so that the ratio of the highest two peaks of the wavelet is approximately $\frac{1}{2}$:

$$\omega_0 = \pi \left(\frac{2}{\ln 2} \right)^{\frac{1}{2}} \approx 5.336. \tag{2.15}$$

For $\omega_0 > 5$, the second term in (2.14) can be neglected. The shape of the Morlet wavelet (2.14) is shown in Fig. 2.3.

The Morlet wavelet (2.14) is an analytical function, i.e., it has only positive frequencies. Consequently, the wavelet coefficients $Wf(s,u)$ in (2.13) are complex

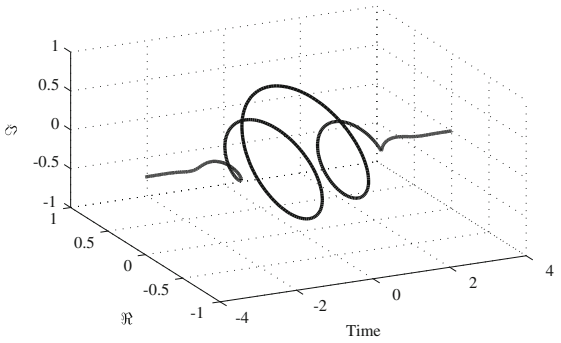

Fig. 2.3 The complex Morlet wavelet

values. As a result, at each time translation u and scale s, the CWT with Morlet wavelet gives the instantaneous amplitude and phase of the analysed signal.

Scale to Frequency Transform for the Morlet Wavelet

The frequencies in CWT (2.13) are represented by scale s, which corresponds to a particular dilatation of the mother wavelet $\psi(t)$. Transforming scale to frequency for the Morlet wavelet is defined as [15]

$$\frac{1}{f} = \frac{4\pi s}{\omega_0 + \sqrt{2 + \omega_0^2}}. \tag{2.16}$$

2.3.4 Cone of Influence

The definition of CWT, given by (2.13), specifies infinite length signals. However, the measured signals always have a finite length. The discontinuities (abrupt changes) at the beginning and the end of the observation window influence the wavelet coefficients in their vicinity. Due to the compact support of the mother wavelets, the distortions influenced by these artificial discontinuities affect only a limited number of wavelet coefficients. The affected wavelet coefficients are located in the so-called *cone of influence* that depends on the selected mother wavelet.

These inaccuracies depend on the part of the mother wavelet support that lies outside of the observation time interval as shown in Fig. 2.4. The hatched areas represent the parts of the wavelet support that span outside of the observation window. It has to be noticed that such areas exist on both sides i.e., at the beginning as well as at the end of the observation window. As the mother wavelet is re-scaled for each analysed frequency, the length of these areas varies. Therefore, only not significantly affected wavelet coefficients should be taken into account for any further analysis.

There is a general rule for selecting the unaffected wavelet coefficients, defined as the e-folding time for the autocorrelation of wavelet power at each scale [15]. This value for the Morlet wavelet reads as

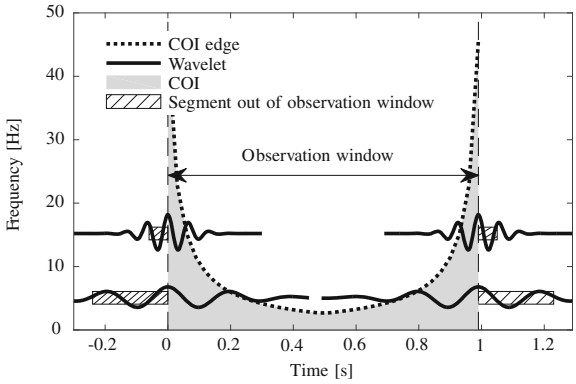

Fig. 2.4 Cone of influence

$$e = s\sqrt{2}. \tag{2.17}$$

The boundary value defined by (2.17) is depicted by the dashed line in Fig. 2.4. The grey area below this boundary line is the cone of influence. The naming *cone* refers to the shape of influenced area's edge over all observed scales. From the shape of the shaded area in Fig. 2.4, it can be noticed that all of the low frequency wavelet coefficients are influenced by the discontinuities occurring on both edges. This in essence means that there are no relevant data for these frequencies. One can overcome this limitation by either using a longer signal or by increasing the sampling frequency of the existing one.

2.3.5 Computationally Efficient CWT with the Morlet Wavelet

The Morlet wavelet allows a computationally efficient implementation of the wavelet transform (2.13). By substituting the mother wavelet $\psi(t)$ with

$$\tilde{\psi}_s(t) = \frac{1}{\sqrt{s}}\psi^*\left(-\frac{t}{s}\right), \tag{2.18}$$

the relation (2.13) transforms into the following convolution:

$$Wf(u,s) = \frac{1}{\sqrt{s}}\int_{-\infty}^{\infty} f(t)\tilde{\psi}_s(u-t)\,dt. \tag{2.19}$$

In the Fourier domain, the convolution (2.19) becomes

$$Wf(u,s) = \frac{1}{2\pi}\int_{-\infty}^{\infty} \hat{f}(\omega)\sqrt{s}\hat{\psi}(s\omega)e^{j\omega u}d\omega, \tag{2.20}$$

where $\hat{f}(\omega)$ is the Fourier transform of the original signal $f(t)$ and $\hat{\psi}(\omega)$ is the Fourier transform of the Morlet wavelet (2.14) [14]:

$$\hat{\psi}(\omega) = \pi^{-\frac{1}{4}} \left(e^{-\frac{(\omega-\omega_0)^2}{2}} - e^{-\frac{\omega^2}{2}} e^{-\frac{\omega_0^2}{2}} \right). \tag{2.21}$$

Therefore, the most computationally demanding process is performed by a simple multiplication in the frequency domain. As a result, the algorithm complexity is governed by the implementation of the FFT algorithm, which has a complexity of $\mathcal{O}(n \log n)$, where n is the number of samples in the signal.

2.3.6 The Lognormal Wavelet

Under certain conditions, the Lognormal wavelet outperforms the Morlet wavelet in terms of time-frequency resolution [11]. The Lognormal wavelet is inline with the logarithmic frequency resolution of the CWT, as it has $\log \omega$ as an argument [11]. The Lognormal wavelet is defined as

$$\hat{\psi}(\omega) = e^{-(\omega_0 \log \omega)^2/2}, \text{ where } \omega > 0. \tag{2.22}$$

The parameter ω_0 can be regarded as the "central frequency" with similar properties as the one of the Morlet wavelet presented in Sect. 2.5. The shape of the lognormal wavelet is shown in Fig. 2.5.

Similarly, as with the Morlet wavelet, the lognormal wavelet allows computationally efficient implementation of the CWT using the same process of calculating the convolution in the frequency domain through FFT. The majority of the results in this book are calculated using the Morlet wavelet unless specified otherwise.

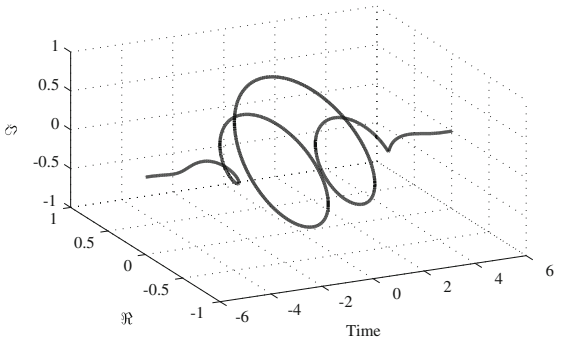

Fig. 2.5 The lognormal wavelet

2.4 Impedance Through Complex Wavelet Coefficients

The result of the CWT analysis of the voltage $u(t)$ and current $i(t)$, with the Morlet wavelet, is a set of complex wavelet coefficients:

$$\begin{aligned} Wi(t, f) &= \Re\{Wi(t, f)\} + j\Im\{Wi(t, f)\}, \\ Wu(t, f) &= \Re\{Wu(t, f)\} + j\Im\{Wu(t, f)\}. \end{aligned} \tag{2.23}$$

Taking into consideration the cone of influence (2.17) and the linearity of the wavelet transform, the impedance can be calculated, similarly as in the case of Fourier transform (2.10), as the following ratio:

$$Z(t, f) = \frac{Wu(t, f)}{Wi(t, f)}. \tag{2.24}$$

The ratio (2.24) provides the value for both the phase and the impedance amplitude in every time-frequency pair. Therefore, by fixing the frequency as $f = f_0$, one is able to estimate the mean impedance value, which is the same as with the calculation through the FFT approach (2.10). However, having the complete time evolution of the complex impedance in every time instance t, one can perform more detailed analysis on the impedance values, for instance estimating the confidence intervals.

2.5 Parameter Selection

For optimal exploitation of the fast EIS method, two parameters have to be specified: (i) the bandwidth of the DRBS excitation f_B and (ii) the central frequency ω_0 of the Morlet mother wavelet. These two parameters influence the sensitivity of the approach with respect to the analysed frequency band, hence their importance for accurate impedance measurements. The parameter selection can be performed in a systematic manner thus guaranteeing optimal performance of the fast EIS approach.

2.5.1 Selection of the DRBS Bandwidth

The rationale behind the selection of the bandwidth parameter f_B is quite intuitive. As shown in Fig. 2.1, the parameter f_B defines the frequency band of the DRBS signal where its frequency spectrum can be considered as sufficiently close to the theoretical flat spectrum of the Gaussian white noise. Therefore, when performing EIS, the frequency band of interest must be contained in the interval $(0, f_b)$. It should be noted that for low frequencies, the previous condition will be always satisfied, which leads to a wrong conclusion that one should just keep the f_B sufficiently high.

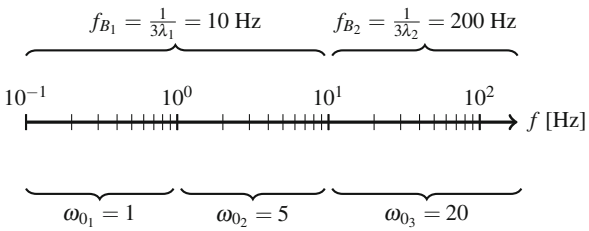

Fig. 2.6 Selection of DRBS bandwidths f_B and Morlet central frequencies ω_0 for a frequency band of interest

Since the energy of the signal is limited, the energy at the individual frequency is proportional to the frequency band f_B. In other words, having high f_B values will cause fast changes in the generated DRBS making it unsuitable for analysing slow responses of the electrochemical system. Therefore, where EIS is performed at low frequencies, the f_B parameter should have low values as well.

From a practical viewpoint, the whole frequency band of interest should be divided into several smaller intervals. The individual bandwith of the employed DRBS excitation should include the maximal frequency of the corresponding interval. One possible way of dividing a frequency band of interest is graphically depicted in Fig. 2.6. The frequency band $[10^{-1}\ 200]$ Hz is divided into two intervals: the low frequency interval, spanning from $[10^{-1}\ 10]$ Hz and the high frequency interval spanning from [10 200] Hz. The corresponding DRBS frequency bands are $f_{B_1} = 10$ Hz and $f_{B_2} = 200$ Hz.

2.5.2 *Influence of the Morlet Wavelet Central Frequency*

The Morlet wavelet central frequency ω_0 determines its time frequency resolution [13, 16]. For smaller ω_0, the shape of the wavelet favours localisation of singular time events, whilst for larger ω_0 more periods of the sine-carrier in the Gaussian window (envelope) make the frequency localisation better.

The broad frequency band and relatively short duration of measured signals raise a problem in relation to the variance of the impedance measurements. The issue is more expressed for lower frequencies. This is due to the fact that at lower frequencies the whole signal contains less periods than the wavelet itself. As a result, there are a lower number of samples that can be employed for estimating the measurement variance. One way of addressing this issue is by lowering the central frequency ω_0.

For the subsequent analysis performed in the following chapters, the observed frequency interval is usually divided into several segments. An example of such a division is presented in Fig. 2.6. Each frequency band is then analysed with the Morlet wavelet whose central frequency is appropriately tuned.

2.6 Accuracy of the Amplitude and Phase Estimates from Wavelet Coefficients

According to the analysis performed by Sejdic et al. [17], estimating the instantaneous amplitude and phase through wavelet coefficients introduces bias. More importantly, the variance and the bias of these estimates depend on the nature of the analysed signal. Due to the discontinuities in the employed DRBS excitation signal, the error in these estimates is further increased.

A simple solution is to make a band-limited version of the DRBS excitation covering only the frequency interval of interest. This can be simply achieved by low-pass filtering the DRBS excitation in such a manner that only the first two lobes of its amplitude spectrum are preserved, i.e., filtering the DRBS signal up to a frequency of $2/\lambda$, as shown in Fig. 2.2.

2.7 Summary

The chapter outlines the fast EIS technique based on discrete random binary sequence excitation and continuous wavelet transform. Unlike the time-averaged impedance values provided by the Fourier transform, the fast EIS technique allows calculation of instantaneous impedance values for an arbitrary set of frequencies. The fast EIS technique is, in the terms of computational complexity, comparable with the Fourier approach. This is achieved by calculating the CWT convolution in the frequency domain.

Optimal impedance results are achieved by using the CWT Morlet mother wavelet. As a result, the fast EIS technique depends on two parameters, the wavelet's central frequency ω_0 and the bandwidth of the excitation signal. The selection of these parameters is straightforward, adding to the applicability of the approach.

Finally, the time-frequency analysis opens the possibility of detailed statistical analysis of the impedance values. Such an analysis is impossible when solely using frequency domain analysis. As it will be shown in the following chapters, the statistical analysis will offer insight on the measurement accuracy as well as open the possibility of using the impedance values for performing various tasks of condition monitoring.

References

1. Yuan, Xiao-Zi, Haijiang Wang, Jian Colin Sun, and Jiujun Zhang. 2007. AC impedance technique in PEM fuel cell diagnosis - a review. *International Journal of Hydrogen Energy* 32: 4365–4380.

2. Wu, Jinfeng, Xiao Zi Yuan, Haijiang Wang, Mauricio Blanco, Jonathan J. Martin, and Jiujun Zhang. 2008. Diagnostic tools in PEM fuel cell research: part I electrochemical techniques. *International Journal of Hydrogen Energy* 33 (6): 1735–1746.
3. Petrone, R., Z. Zheng, D. Hissel, M.C. Péra, C. Pianese, M. Sorrentino, M. Becherif, and N. Yousfi-Steiner. 2013. A review on model-based diagnosis methodologies for PEMFCs. *International Journal of Hydrogen Energy* 38 (17): 7077–7091. doi:10.1016/j.ijhydene.2013.03.106.
4. Zheng, Z., R. Petrone, M.C. Péra, D. Hissel, M. Becherif, C. Pianese, N. Yousfi-Steiner, and M. Sorrentino. 2013. A review on non-model based diagnosis methodologies for PEM fuel cell stacks and systems. *International Journal of Hydrogen Energy* 38 (21): 8914–8926. doi:10.1016/j.ijhydene.2013.04.007.
5. Niya, Seyed Mohammad Rezaei, and Mina Hoorfar. 2013. Study of proton exchange membrane fuel cells using electrochemical impedance spectroscopy technique - a review. *Journal of Power Sources* 240: 281–293. doi:10.1016/j.jpowsour.2013.04.011.
6. Lasia, Andrzej. 2014. *Electrochemical impedance spectroscopy and its applications*. New York: Springer. doi:10.1007/978-1-4614-8933-7.
7. Yuan, Xiao-Zi, Chaojie Sons, Haijiang Wang, and Jiujun Zhang. 2010. *Electrochemical impedance spectroscopy in PEM fuel cells, fundamentals and applications*. London: Springer.
8. Isermann, Rolf, and Marco Münchhof. 2011. *Identification of dynamic systems: an introduction with applications*. Advanced textbooks in control and signal processing. Berlin: Springer. doi:10.1007/978-3-540-78879-9.
9. Davies, W.D.T. 1970. *System identification for self-adaptive control*. New York: Wiley.
10. Ljung, Lennart. 1999. *System identification: theory for the user*, 2nd ed. Prentice-Hall information and system sciences series. Upper Saddle River: Prentice-Hall.
11. Iatsenko, Dmytro. 2015. *Nonlinear mode decomposition*. Springer theses. Springer International Publishing.
12. Mallat, Stéphane. 2008. *A wavelet tour of signal processing: the sparse way*, 3rd ed. Amsterdam: Elsevier Academic Press.
13. Stefanovska, Aneta, and Maja Bračič. 1999. Physics of the human cardiovascular system. *Contemporary Physics* 40 (1): 31–55.
14. Daubechies, Ingrid. 1992. *Ten lectures on wavelets*. CBMS-NSF regional conference series in applied mathematics. Philadelphia: Society for Industrial and Applied Mathematics.
15. Torrence, Christopher, and Gilbert P. Compo. 1998. A practical guide to wavelet analysis. *Bulletin of the American Meteorological Society* 79: 61–78.
16. Musizza, Bojan, Aneta Stefanovska, Peter V.E. McClintock, Milan Paluš, Janko Petrovčič, Samo Ribarič, and Fajko F. Bajrović. 2007. Interactions between cardiac, respiratory and EEG-δ oscillations in rats during anaesthesia. *The Journal of Physiology* 580 (1): 315–326. doi:10.1113/jphysiol.2006.126748.
17. Sejdic, E., I. Djurovic, and L. Stankovic. 2008. Quantitative performance analysis of scalogram as instantaneous frequency estimator. *IEEE Transactions on Signal Processing* 56 (8): 3837–3845. doi:10.1109/TSP.2008.924856.

http://www.springer.com/978-3-319-53389-6

Fast Electrochemical Impedance Spectroscopy
As a Statistical Condition Monitoring Tool

Boškoski, P.; Debenjak, A.; Mileva Boshkoska, B.

2017, XIII, 83 p. 43 illus., 11 illus. in color., Softcover
ISBN: 978-3-319-53389-6